View Article Online / Journal Homepage / Table of Contents for this issue
Dynamic Article Links

Nanoscale

Cite this: *Nanoscale*, 2012, **4**, 7517

www.rsc.org/nanoscale

PAPER

Self-assembled GaN quantum wires on GaN/AlN nanowire templates†

Jordi Arbiol,*[a] Cesar Magen,[bc] Pascal Becker,[d] Gwénolé Jacopin,[e] Alexey Chernikov,[f] Sören Schäfer,[f] Florian Furtmayr,[dg] Maria Tchernycheva,[e] Lorenzo Rigutti,‡[e] Jörg Teubert,[d] Sangam Chatterjee,[f] Joan R. Morante[h] and Martin Eickhoff*[d]

Received 6th August 2012, Accepted 5th October 2012
DOI: 10.1039/c2nr32173d

Published on 09 October 2012. Downloaded by UNIVERSITAT GIESSEN on 24/01/2014 13:19:43.

We present a novel approach for self-assembled growth of GaN quantum wires (QWRs) exhibiting strong confinement in two spatial dimensions. The GaN QWRs are formed by selective nucleation on $\{11\bar{2}0\}$ (*a*-plane) facets formed at the six intersections of $\{1\bar{1}00\}$ (*m*-plane) sidewalls of AlN/GaN nanowires used as a template. Based on microscopy observations we have developed a 3D model explaining the growth mechanism of QWRs. We show that the QWR formation is governed by self-limited pseudomorphic growth on the side facets of the nanowires (NWs). Quantum confinement in the QWRs is confirmed by the observation of narrow photoluminescence lines originating from individual QWRs with emission energies up to 4.4 eV. Time-resolved photoluminescence studies reveal a short decay time (~120 ps) of the QWR emission. Capping of the QWRs with AlN allows enhancement of the photoluminescence, which is blue-shifted due to compressive strain. The emission energies from single QWRs are modelled assuming a triangular cross-section resulting from self-limited growth on *a*-plane facets. Comparison with the experimental results yields an average QWR diameter of about 2.7 nm in agreement with structural characterization. The presented results open a new route towards controlled realization of one-dimensional semiconductor quantum structures with a high potential both for fundamental studies and for applications in electronics and in UV light generation.

A Introduction

Semiconductor quantum wires (*i.e.* nanostructures exhibiting confinement in two spatial dimensions) present a strong interest both for fundamental studies and for electronic as well as photonic applications.[1–3] However, while quantum wells (systems with confinement in one dimension) and quantum dots (systems with confinement in 3 dimensions) are widely used in optoelectronic devices, the quantum wires (QWRs) are up to now much less studied. This is mainly due to the challenge related to the QWR synthesis. Indeed, in order to observe confinement effects, the lateral dimensions have to be reduced below the typical dimensions of the excitonic wavefunctions which are on the order of a few nanometers,[4] *i.e.* the controlled synthesis of quantum wires (QWRs) or quantum dots is required. Concerning the former, presently only a few reports on the growth of semiconductor QWRs (with different diameters) exist: CdTe,[5] CdSe (5–20 nm),[6] InP (3–11 nm),[7] Ge (7–30 nm),[8] and Si (4–5 nm)[9] have been synthesized from solutions. GaAs QWRs on the (100) surfaces of (111) limited ridge structures, formed by photolithography and reactive ion etching, have been fabricated by molecular beam epitaxy (MBE).[10] A similar method has been used for MBE-growth of InGaAs QWRs on InP ridge structures.[11] Growth of V-groove GaAs QWR-like nanostructures by MBE employing anisotropic surface kinetics and exciton transfer between two QWRs separated by AlGaAs barriers was also reported. A similar approach has recently been reported for ZnO QWRs.[12,13] Also, using the cleaved edge overgrowth technique, GaAs quantum wire lasers with the one dimensional confinement region formed at the T-shaped intersections of 7 nm wide GaAs

[a]*Institució Catalana de Recerca i Estudis Avançats (ICREA) and Institut de Ciència de Materials de Barcelona, ICMAB-CSIC, Campus de la UAB, E-08193 Bellaterra, CAT, Spain. E-mail: arbiol@icrea.cat*
[b]*Laboratorio de Microscopías Avanzadas, Instituto de Nanociencia de Aragon-ARAID, Universidad de Zaragoza, 50018 Zaragoza, Spain*
[c]*Departamento de Física de la Materia Condensada, Universidad de Zaragoza, 50009 Zaragoza, Spain*
[d]*I. Physikalisches Institut, Justus-Liebig-Universität Gießen, Heinrich-Buff-Ring 16, DE-35392 Gießen, Germany. E-mail: eickhoff@physik.uni-giessen.de*
[e]*Institut d'Electronique Fondamentale, University of Paris Sud XI, UMR 8622 CNRS, 91405 Orsay, France*
[f]*Faculty of Physics and Materials Science Center, Philipps Universität Marburg, Renthof 5, DE-35032 Marburg, Germany*
[g]*Walter Schottky Institut, Technische Universität München, Am Coulombwall 4, DE-85748 Garching, Germany*
[h]*Catalonia Institute for Energy Research, IREC. 08930 Sant Adrià del Besòs, Spain and Department d'Electrònica, Universitat de Barcelona, 08028 Barcelona, Spain*

† Electronic supplementary information (ESI) available: Additional analyses on the QWR structure and morphology, plan view microscopy of the heterostructures, details on simulations, strain and direct polarity analyses. See DOI: 10.1039/c2nr32173d

‡ Present address: Groupe de Physique des Matériaux, UMR CNRS 6634, University of Rouen, 76801 St Etienne du Rouvray, France.

View Article Online

Published on 09 October 2012. Downloaded by UNIVERSITAT GIESSEN on 24/01/2014 13:19:43.

quantum wells grown along the [001] crystal axis and after an *in situ* cleave along the [110] crystal axis have been realized.[14]

In group III-nitride materials (III-Ns) the formation of GaN QWRs has only been reported in ref. 15, where self-assembled growth of GaN QWR structures with a width of approximately 35 nm and a height between 1.5 and 3 nm on AlN/6H-SiC substrates with anisotropic strain as the driving force has been shown. In a recent theoretical study, QWRs formed along the edges of prismatic shaped nanowires (NWs) have been proposed for the investigation of physical effects arising from the one-dimensionality of these structures, *e.g.*, Aharanov–Bohm oscillations or Landau-level formation.[16] In that work it is shown, how axially extended quasi one-dimensional confined states are formed at the edges of spatially bent quantum wells formed by the lower band-gap material of a core–shell multi-heterostructure, *e.g.*, InGaN/GaN. Despite the strong research effort on the self-assembled growth of III-N NWs and NW heterostructures, self-organized synthesis of QWRs with lateral dimensions below 10 nm has not yet been demonstrated for this material system.

Presently NWs are employed in order to improve the performance of existing device architectures, in the case of group III-nitrides this is mainly an increase in the efficiency of opto-electronic emitters by suppression of defect-induced degradation mechanisms.

New device concepts based on the exploitation of quantum effects or specific properties arising from the one-dimensional geometry of nanostructures are typically ignored as, from an electronic point of view, most NWs are still bulk-like.

Here, we propose a novel approach for an efficient synthesis of QWRs using a self-assembled AlN/GaN NW core–shell structure as a template. AlN/GaN NW structures similar to the templates employed here have also been reported in earlier works.[17] The self-assembled multiple GaN QWR-structures are achieved at the edges of prismatic NWs by plasma-assisted MBE (PAMBE). We show that the self-assembly process of GaN QWRs on the six edges of intersecting AlN $\{1\bar{1}00\}$-planes which form the lateral facets of a GaN/AlN NW heterostructure is driven by orientation-selective nucleation on the NW sidewalls. Analysis by aberration-corrected atomic-resolution *Z*-contrast scanning transmission electron microscopy (STEM) reveals that GaN QWRs with a projected lateral extension down to a single monolayer (ML) are pseudomorphically grown on the six AlN $\{11\bar{2}0\}$-edges axially along the [0001] direction. Micro-photoluminescence studies of single NWs reveal narrow emission lines in the energy range between 3.7 and 4.4 eV originating from individual QWRs.

Ensemble PL data of such QWRs show a red-shift of the average emission energy with increasing amount of deposited GaN as well as a blue-shift upon coverage with an additional AlN shell due to modification of the strain distribution. The controlled growth of one-dimensional QWR structures opens the way to the investigation of new physical effects and novel optoelectronic applications as well as to the enhancement of UV emission from III-N optoelectronic devices for new lighting technologies.

B Experimental

AlN/GaN NW heterostructures were grown by PAMBE under nitrogen-rich growth conditions, which promote quasi one-dimensional growth along the *c*-direction without requiring any external catalyst.[18] It was recently reported that the anisotropic growth rate is related to surface thermodynamics and nucleation rather than originating in anisotropic adatom mobilities.[19] This indicates that one-dimensional growth specifically occurs when the lateral NW surfaces are $\{1\bar{1}00\}$-facets. As a consequence, different nucleation properties are expected for the growth on $\{11\bar{2}0\}$- or related facets formed at the intersections of the lateral $\{1\bar{1}00\}$-planes.

Here, GaN NWs with a diameter of 25–50 nm and a height between 130 and 300 nm were grown as the base part of AlN/GaN NW heterostructures on low-resistivity Si(111) substrates at a temperature of 775 °C and 770 °C according to the growth process described elsewhere.[20,21] The applied beam-equivalent pressure of the Ga-cell (BEP_{Ga}(base)) as well as the growth time t_{base} and other growth parameters are summarized in Table 1. Whereas the metals were supplied by thermal effusion cells, nitrogen was introduced by a radio-frequency plasma source. Nitrogen-rich growth conditions (V/III $\approx$ 4–6 compared to a GaN layer) were applied to form self-assembled NWs. In a second step, AlN was deposited on top of the GaN base with the growth time t_{AlN}. Under the applied growth conditions, lateral growth of AlN and a resulting widening of the AlN part with respect to the GaN-base are expected. While the GaN NW base exhibits a prismatic shape with lateral facets being mainly formed by $\{1\bar{1}00\}$-planes, the deposition of an AlN layer leads to "softening" of these lateral facets, *e.g.*, by exposure of $\{11\bar{2}0\}$-planes at the six intersections.[20] In a third step, a thin layer of GaN was deposited (growth time t_{QWR}). For samples A–D this step was carried out at four different beam equivalent pressures of the Ga effusion cell (BEP_{Ga}(QWR)) to assess the growth window for QWR formation on the edges ($\{11\bar{2}0\}$-facets) without nucleation on the $\{1\bar{1}00\}$-facets themselves. For samples E and F an additional AlN capping layer was deposited in the final step (growth time t_{AlN}, *cf.* Table 1).

Atomic-resolution aberration-corrected high angle annular dark field (HAADF or Z-contrast) STEM imaging was performed on a probe-corrected FEI Titan 60–300 keV microscope operated at 300 keV. In order to prepare the samples for TEM observation, the NWs were removed mechanically and dispersed on a holey carbon copper grid as described elsewhere.[22] 3D atomic models of the QWRs were constructed using the Rhodius software,[23] widely used to model NW complex nanostructures.[24] For time-resolved photoluminescence (TRPL) measurements, a 100 fs, 80 MHz repetition rate Ti:sapphire laser frequency-tripled to 4.43 eV was used as excitation source. The pump density per pulse was set to 1.4×10^{12} photons per cm^2 in the 25 μm FWHM pump spot. The samples were mounted inside a He-flow cryostat and the measurements were performed at a lattice temperature of 10 K. The PL signal was detected using the standard streak-camera setup,[25] with the spectral and temporal resolutions of 0.2 nm and 10 ps, respectively.

Micro photoluminescence (μ-PL) measurements were carried out in a setup described in ref. 26. Single NW PL was excited using a frequency-doubled cw Ar^+ laser at 244 nm after dispersing the NWs on an oxidized silicon substrate. The laser was focused on the substrate surface in a spot with a diameter of $\sim$3 μm by means of a UV microscope objective with a numerical aperture of 0.4, the excitation power was in the μW range. PL spectra were recorded at a temperature of 4 K using a HR460

 This journal is © The Royal Society of Chemistry 2012

View Article Online

Published on 09 October 2012. Downloaded by UNIVERSITAT GIESSEN on 24/01/2014 13:19:43.

Table 1 Growth conditions of the NW heterostructures analysed in this work

Sample	BEP_{Ga}(base) [mbar]	BEP_{Al} [mbar]	BEP_{Ga}(QWR) [mbar]	t_{AlN} [s]	t_{base} [min]	t_{QWR} [s]	T_{sub} [°C]
(A)	2.1×10^{-7}	3.5×10^{-7}	3.8×10^{-7}	780	70	180	775
(B)	2.1×10^{-7}	3.5×10^{-7}	2.7×10^{-7}	780	70	180	775
(C)	2.1×10^{-7}	3.5×10^{-7}	1.9×10^{-7}	780	70	180	775
(D)	2.1×10^{-7}	3.5×10^{-7}	1.4×10^{-7}	780	70	180	775
(E)	3×10^{-7}	3.5×10^{-7}	3.0×10^{-7}	560	70	160	770
(F)	3×10^{-7}	3.5×10^{-7}	4.5×10^{-7}	560	70	160	770

spectrometer with a 600 grooves per mm grating and a CCD camera. The energy resolution of the setup during these experiments was kept in the range of 1 meV.

C Results and discussion

Structural analysis of the NW heterostructures by HAADF STEM imaging (Fig. 1a–c) shows that the deposition of the first AlN part results in a core–shell heterostructure with consequent formation of a lateral shell on the $\{1\bar{1}00\}$ GaN side facets.[20] A lateral growth rate of 0.2 Å s^{-1}, *i.e.* 22% of the axial growth rate (0.1 nm s^{-1}) was extracted.

For sample A we find that during the second GaN deposition a thin GaN layer with an average thickness of 5 nm is deposited on the top of the AlN part. A considerable surface distortion is attributed to the high growth temperatures and the strongly N-rich growth conditions applied for samples A–D.

While during the growth of this thin GaN layer no deposition on the $\{1\bar{1}00\}$ sidewalls is found, nucleation of GaN on the six edges formed at the intersection between the $\{1\bar{1}00\}$-facets of the AlN part is observed (*cf.* Fig. 1a–e and 3D atomic model in Fig. 3). Atomic resolution analysis, displayed in Fig. 1d and e, clearly shows the 7 $\{1\bar{1}00\}$ monolayers (MLs) projected diameter of the QWR which is equivalent to a 7 ML $\{11\bar{2}0\}$ diameter of the QWR (Fig. S7, ESI†). It should be noticed that the QWRs can be damaged by the electron beam after less than one minute. They start to decompose and become amorphous, forming discontinuities along the QWR growth axis as shown in Fig. S1a and b (ESI†).

To enhance the stability of the QWRs and to suppress quenching of the PL intensity by surface adsorbates,[27,28] QWR samples capped by a second lateral AlN shell were realized (samples E and F). Employing the observed high selectivity of GaN nucleation on *m*- and *a*-plane AlN, these samples were grown at a higher BEP_{Ga} and slightly lower substrate temperatures (*cf.* Table 1). The BEP_{Ga} was a factor of 1.5 higher for sample F compared to sample E and the AlN cap layer for both samples was grown under the same conditions as the first AlN part.

STEM analysis of the resulting NW structures (sample F) visualizes the QWRs on the $\{11\bar{2}0\}$ AlN shell edges, shown in Fig. 2. As in the case of samples A–D, lateral AlN deposition on the $\{1\bar{1}00\}$ GaN side facets during growth of the first AlN barrier is also promoted, creating an envelope shell around the core (*cf.* Fig. S2, ESI†). During the second GaN deposition nucleation on the six lateral $\{11\bar{2}0\}$ edges of the AlN shell along the [0001] direction occurs (*cf.* results in Fig. 2 and 3D atomic model in Fig. 6). Due to the modified growth conditions, the axial growth rate during the second GaN deposition is enhanced, as visualized by the 20 nm thick GaN part with sharp interfaces between the first and the second AlN layers in the axial direction. At the same time, no systematic increase of the size of the QWRs was found,

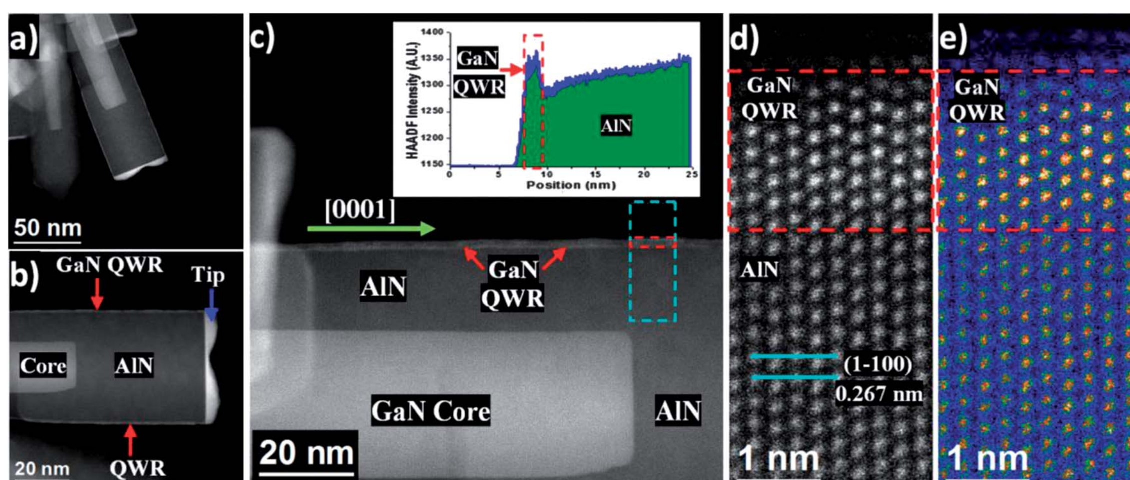

Fig. 1 (a) Low magnification Z-contrast image of one of the NW heterostructures containing the QWRs in sample A. The brightest contrast corresponds to the GaN and the darker to the AlN. (b) HAADF STEM details showing the lateral QWRs (pointed with red arrows). (c) Atomic resolution aberration corrected HAADF STEM image showing the 7 $(1\bar{1}00)$ monolayer projected diameter of the QWR. Inset corresponds to the intensity profile obtained along the dashed cyan box in (c). (d) Z-contrast magnified details of one of the GaN QWRs, brightest atomic columns correspond to the ones containing Ga atoms. (e) Same as (d) but applying false colour to enhance the contrast.

Published on 09 October 2012. Downloaded by UNIVERSITAT GIESSEN on 24/01/2014 13:19:43.

pointing towards a self-limiting growth mechanism for the QWR structures. During the growth of the AlN cap layer the finite lateral growth rate of AlN causes coverage of the GaN QWRs (Fig. 2a and b), leading to an enhanced stability of the QWR structures and allowing optical and structural characterization by PL spectroscopy and electron microscopy without damage.

QWRs of a projected diameter of 2 $\{1\bar{1}00\}$ MLs (corresponding to 2 $\{11\bar{2}0\}$ MLs) were created on one edge of an AlN barrier after axial deposition of a 20 nm top GaN layer in the *c*-direction (sample analysed in Fig. 2). It has to be noted that the projected size of the QWR diameter on the different edges of one NW template shows variations of more than 50%, indicating that it is not primarily determined by the applied Ga-flux. In Fig. S3 (ESI†) we show the different edge QWRs of the same sample, after slightly rotating the NW out of the $[11\bar{2}0]$ zone axis in order to avoid overlapping and give a 3-dimensional (3D) sense of the heterostructure. Whereas the projected diameter of the QWRs on one NW varies, each QWR exhibits a high regularity and homogeneity. It is possible to identify even a single GaN ML QWR (Fig. S4†), emphasizing on one hand the lower limit for GaN deposition on the AlN shell edges and, on the other hand, the power of the atomic resolution aberration-corrected HAADF-STEM imaging (more details in the ESI†).

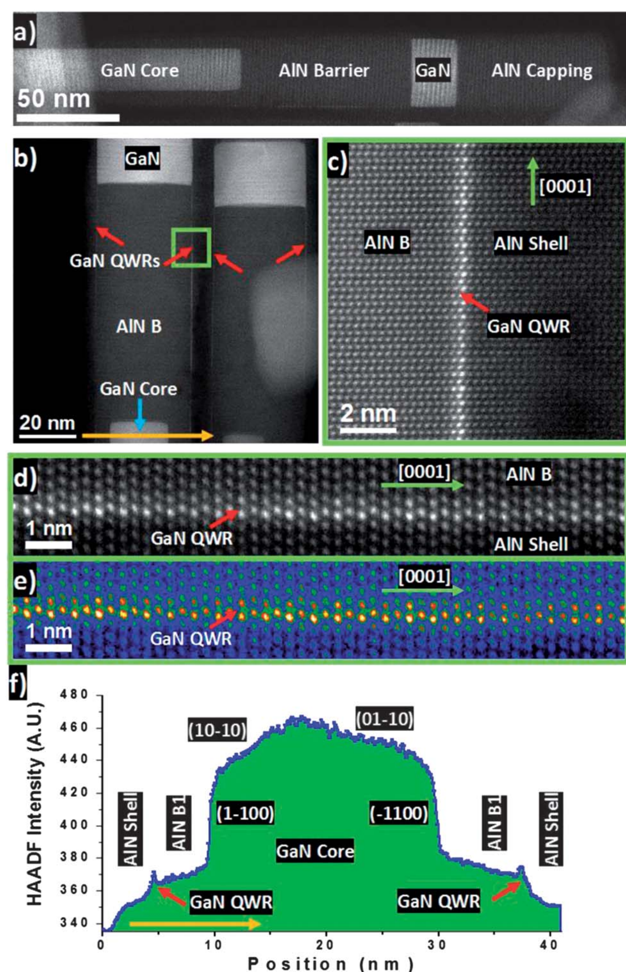

Fig. 2 (a) Low magnification HAADF STEM view of one of the NW heterostructures containing the QWRs in sample F. The brightest contrast corresponds to the GaN and the darker to the AlN. (b) HAADF STEM imaging details showing the lateral QWRs (pointed with red arrows). (c) Atomic resolution HAADF STEM image showing the 2 $(1\bar{1}00)$ ML projected diameter of the QWR on the left. (d) Z-contrast magnified details of one the GaN QWRs, brightest atomic columns correspond to the ones containing Ga atoms. (e) Same as (d) but applying false color to enhance the contrast. (f) Intensity profile obtained along the orange arrow in (b). Notice that we can distinguish all the features labeled on the HAADF image.

Additional strain measurements demonstrate partial relaxation of the AlN shell and barrier *versus* the NW GaN core and top layer (*cf.* Fig. S5a–d, ESI†). The relaxation mechanism occurs through formation of misfit dislocations.[20] Direct polarity measurements[29,30] reveal that both GaN and AlN are of N-face polarity, as reported elsewhere[29] and shown also in Fig. S5 (ESI†) by the aberration-corrected annular bright field (ABF) STEM imaging technique.

We exclude strain anisotropy as the driving force for QWR formation in contrast to the results for GaN quantum wires on the *m*-plane AlN/6H-SiC with thin AlN buffer layers reported in ref. 15. Instead, we find that selective nucleation on the $\{11\bar{2}0\}$- or related facets initiates QWR growth. This is most likely due to differences in thermodynamic stability or nucleation probability,[19] as we do not observe nucleation on the $\{1\bar{1}00\}$ AlN side walls in the whole investigated regime of Ga-flux. As a direct consequence the diameter of the nucleation edge facet determines the diameter of the QWR cross-section. This is further confirmed by the wide distribution of QWR sizes that is observed even on a single NW which indicates that the size cannot only depend on the applied BEP_{Ga}(QWR) during growth, but is most likely determined by a self-limiting growth mechanism that determines the QWR size on each nucleation facet of one NW. As QWR nucleation occurs selectively on the $\{11\bar{2}0\}$-facets (or similar) of the first AlN shell, the growth proceeds along the $[11\bar{2}0]$-direction (or similar). Based on HAADF STEM analysis here and the results reported in ref. 20, it can be assumed that under the N-rich growth conditions applied here nucleation does not occur on GaN and AlN $\{1\bar{1}00\}$-facets, which therefore form the lateral boundaries during growth (*cf.* Fig. 3 and S7, ESI,† and animated 3D atomic models elsewhere).[31] Consequently, QWR growth will be suppressed as soon as the outer surfaces are completely formed by $\{1\bar{1}00\}$-facets and the maximum QWR diameter is determined by the initial width and the exact orientation of the AlN-facet for QWR nucleation, resulting in a broad distribution of QWRs cross-sections, whereas the actual (triangular) shape is determined by the orientation of the involved crystal facets (*cf.* inset in Fig. 6b). In order to control the size and the homogeneity of the resulting QWRs the growth conditions, particularly the diameter and the homogeneity, of the inner AlN shell have to be carefully controlled.

TRPL analysis of the NW ensemble reveals the optical fingerprint of the QWRs (Fig. 4). A typical streak-camera image of the NW ensemble of sample F is displayed in Fig. 4. It clearly shows the different decay dynamics of the emission related to the NW base and to the QWRs, respectively. The temporal and spectral profiles integrated over the complete detection window are shown below and on the right-hand side, respectively.

Two different emission bands are observed: the lower-energy part around 3.5 eV is attributed to GaN emission from the NW base[32] that is slightly blue-shifted due to compressive strain

 This journal is © The Royal Society of Chemistry 2012

Published on 09 October 2012. Downloaded by UNIVERSITAT GIESSEN on 24/01/2014 13:19:43.

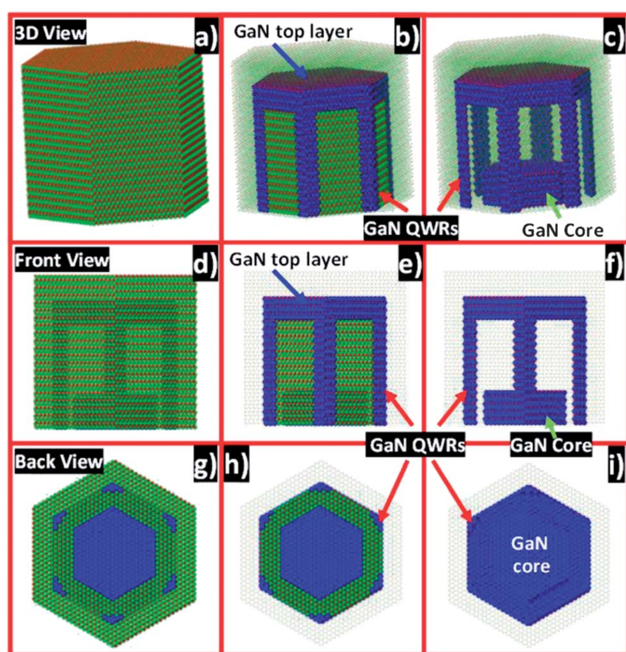

Fig. 3 (a–c) 3D atomic model of the QWRs grown on the 6 truncated edges of a GaN–AlN NW template (visualized in 3D). (d–f) The same model but visualized along the $[11\bar{2}0]$ axis (lateral view), equivalent to the axis observed in the HAADF STEM images. (g–i) The same model on the back view (along the $[000\bar{1}]$ growth axis, with N-polarity). The lateral facets of the projected hexagonal prisms correspond to $\{1\bar{1}00\}$ planes. (a), (d), and (g) are modeled with a compact view of the external AlN shell. (b), (e), and (h) have been modeled by fading the AlN external shell, to allow visualization of the 6 inner QWRs and the top GaN layer. (c), (f), and (i) have been modeled by fading also the inner AlN shell, allowing even the visualization of the GaN inner NW core (see also Fig. S7, for different ML diameter QWR models, ESI†). See also the following link for the corresponding animated 3D atomic simulations: http://www.icmab.cat/gaen/research/165.

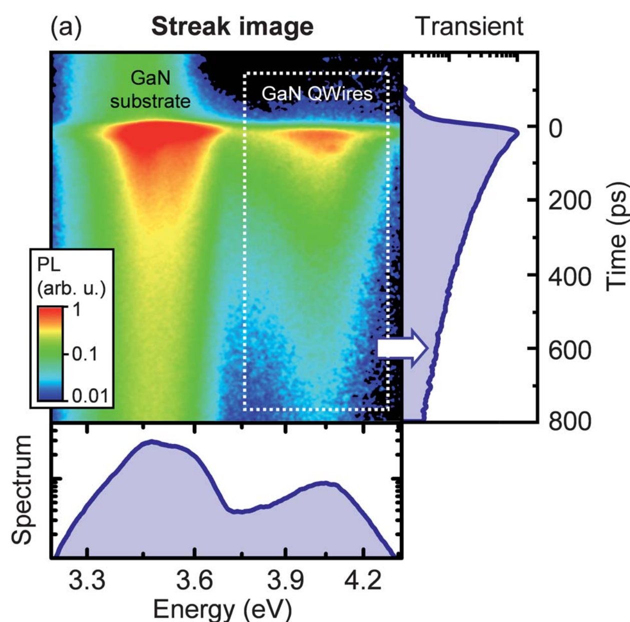

Fig. 4 Time resolved ensemble PL analysis of the sample F. The streak camera image demonstrates the different characteristics of the QWR related emission and shows the extracted spectrum obtained by integration over the first 100 ps (bottom) as well as the time-resolved integrated PL intensity of the spectral range marked in the camera-image (right).

caused by the presence of the AlN shell,[33] possibly it also contains contributions from the thin GaN tip. The emission band between 3.85 eV and 4.05 eV originates from the QWR ensemble. It is shifted by energies up to 0.5 eV towards higher energies due to the large quantum confinement in the QWR. It is also influenced by the three dimensional compressive stress caused by pseudomorphic growth on a $\{11\bar{2}0\}$ AlN facet and by the AlN capping layer (see ESI, Fig. S5†). This emission band cannot originate from states confined along the polar *c*-direction as its emission energy is not compatible with the analyzed size of GaN inclusions along the growth axis.

The QWR emission around 4 eV features a PL decay time of 120 ps down to the $1/e$ of its initial intensity, followed by a slower decay. This is significantly shorter than the emission of the GaN NW around 3.5 eV characterized by a decay time of 250 ps.

Previously, a non-monoexponential decay of the PL intensity to $1/e$ of its initial value after 180 ps was reported for GaN quantum wires.[15] The faster decay observed for the QWRs in the present study is attributed to a significantly smaller cross-section of the QWRs leading to a higher overlap of the carrier wave functions.

The low-temperature ensemble-PL spectra of samples A–F are compared in Fig. 5. The emission around 3.4 eV can be assigned to the GaN NW base and in the case of samples E and F to the 20 nm GaN inclusion in the top part of the NW, according to Fig. 2a. For the latter, the high-energy shoulder is shifted to higher energies if the excitation energy is increased (not shown), indicating the influence of polarization induced internal electric fields. In contrast, the energy of the QWR-related emission remains constant, pointing towards confinement on a non-polar surface. For samples of the first series, the energy of the QWR-related emission band increases with decreasing Ga-flux, *i.e.*,

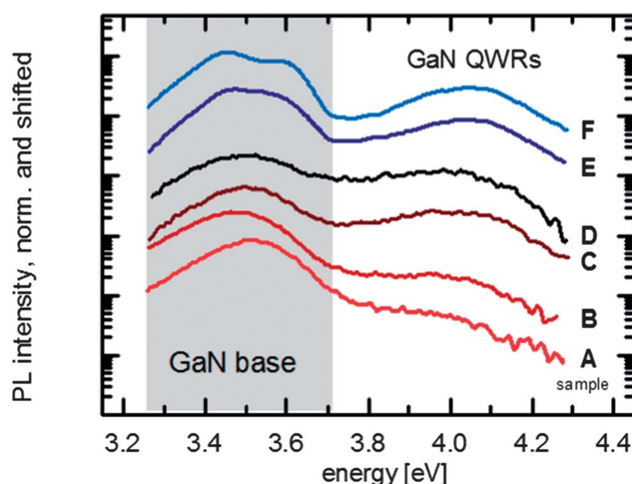

Fig. 5 Low temperature photoluminescence spectra of NW ensembles containing QWRs on the samples grown under different growth conditions recorded at $T = 10$ K. A blue-shift of the emission energy and an enhancement of the emission intensity due to the presence of the AlN capping layer in samples E and F are observed.

Published on 09 October 2012. Downloaded by UNIVERSITAT GIESSEN on 24/01/2014 13:19:43.

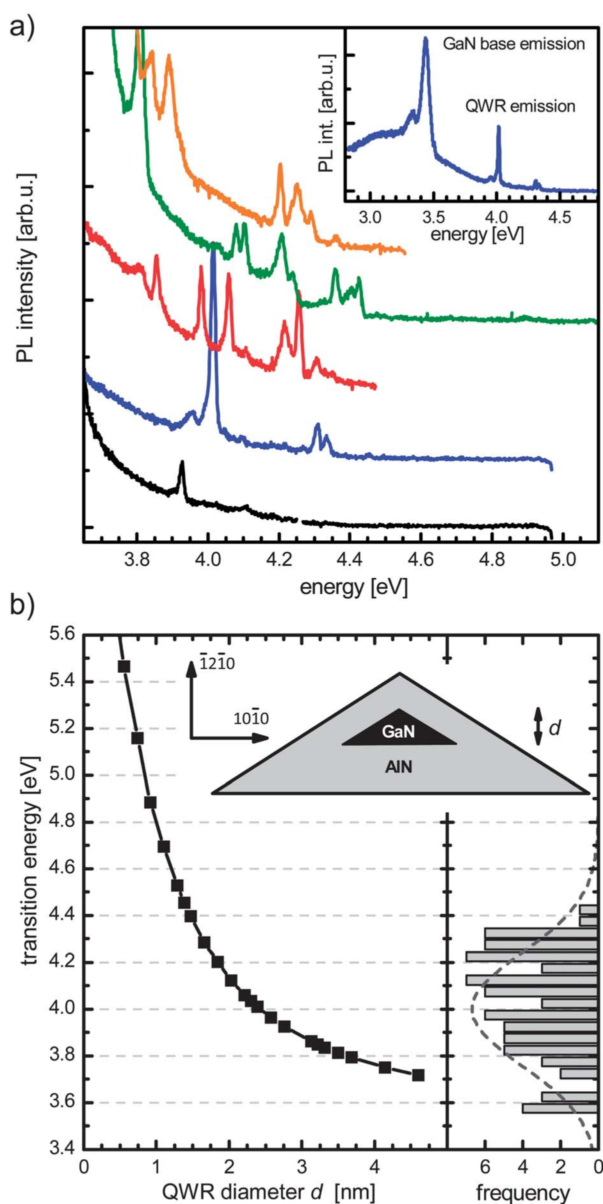

Fig. 6 (a) High energy range of low temperature ($T = 4$ K) PL spectra from single NW measurements. The distinct peaks in that range are assigned to emission from single QWRs. The inset shows an overview over the whole measurement range containing the more intense emission from the GaN base for comparison. (b) Left panel: calculated dependence of the QWR emission energy as a function of the QWR diameter according to the geometry shown as a cross-section for a single QWR in the inset. Right panel: histogram of QWR emission energies from 24 single NW spectra. By comparison to the calculations an average QWR diameter between 1.7 nm and 2.5 nm is obtained.

with decreasing average size of the QWRs due to the increase of the confinement energy. The only exception is the sample with the lowest amount of deposited GaN (sample D). Here, the apparent decrease in emission energy is attributed to laser-induced damage that causes strain relaxation by island formation, as it was also observed due to electron beam damage (Fig. S6, ESI†). A shift of the emission band by approximately 100 meV towards higher energies is observed after deposition of an AlN capping layer in samples E and F. This is mainly attributed to the modification of the mechanical stress distribution caused by the three-dimensional embedment of the QWRs in the AlN shell, compared to the biaxial compressive stress of the uncapped QWRs. The assignment is supported by the simulations presented below. At the same time, we observe an increase of the emission intensity relative to the emission from the GaN base and a slight increase of the $1/e$ decay time from about 60 ps for the uncapped sample to 120 ps for the capped one, demonstrating the decreasing influence of non-radiative surface recombination caused by surface defects and/or surface adsorbates[27,28] upon deposition of the AlN capping layer.

To obtain further insight into the QWR emission characteristics we have performed μ-PL analysis of single NWs containing up to six QWRs from sample F.

The inset of Fig. 6a shows a typical single NW spectrum characterized by an emission line at 3.43 meV that originates from the GaN NW base and contains contribution from the 20 nm GaN disc. The width of this emission line that differs in its actual shape from wire to wire was 50 meV on average. At higher energies, single emission lines with an average width of 10 meV were observed. The number of these emission lines ranges between 2 and 6 for each NW and their shape as well as the transition energies differ between individual NWs as depicted in the example spectra of the above band gap spectral range of five different NWs in Fig. 6a.

We attribute the narrow emission lines to emission from single QWRs. Wider emission lines might originate from emission of two or more QWRs with similar emission energy or from size fluctuations of the QWRs due to different widths of the nucleation facet. Thickness fluctuations of the AlN capping layer also cause differences in emission energy of different QWRs on one and the same NW or on different NWs (*cf.* Fig. S8, ESI†).

In Fig. 6b (right panel), the distribution of QWR emission energies obtained from analysis of 24 different single NWs is depicted, covering a wide range of emission energies from 3.7 to 4.4 eV. We have also included the results of simulations using nextnano^3, a three-dimensional Poisson–Schrödinger solver with full consideration of mechanical strain including free strain relaxation at the nanowire surface.[34] These yield an estimate for the QWR emission energies, which is in excellent agreement with the observed ensemble PL spectra (Fig. 4 and 5). Here, the QWRs have been modelled in a two dimensional calculation with a triangular cross-section according to the growth model described above, with the $(11\bar{2}0)$ plane forming the base of the triangle and the $\{1\bar{1}00\}$ planes forming the sidewalls (*cf.* inset in Fig. 6b). In that case the size of the QWR cross-section is fully defined by the size of the $(11\bar{2}0)$ nucleation plane formed at the intersections of two neighbouring $\{1\bar{1}00\}$ planes. In Fig. 6b (left panel) the calculated transition energies are shown as a function of the base diameter of the triangular QWR cross-section for three dimensionally compressed QWRs obtained by deposition of an AlN capping corresponding to the single NW PL measurements displayed in Fig. 6a. The thickness of the outer AlN-shell due to the AlN capping layer was 10 nm and the effect of the QWR dimensions on the exciton binding energy has explicitly been considered using a variational approach.[34]

By comparison of simulation and experiment we obtain a distribution of the QWR diameter between 1.7 and 2.5 nm which is

 This journal is © The Royal Society of Chemistry 2012

Published on 09 October 2012. Downloaded by UNIVERSITAT GIESSEN on 24/01/2014 13:19:43.

in good agreement with the HRTEM analysis and strongly corroborates the proposed growth model. In addition, we have investigated the blue-shift due to the presence of the AlN capping layer by varying the thickness of the outer AlN shell in the simulations from 1 nm to 20 nm. We find an increase of the transition energy with increasing AlN-shell thickness due to different strain states of the QWR with saturation above an AlN-shell thickness of ~10 nm (*cf.* Fig. S8, ESI†). From these results the blue-shift due to the presence of the AlN capping layer was determined to approximately 90 meV, which is in excellent agreement with the values extracted from the ensemble PL analysis in Fig. 5.

The numerical results further support the assignment of the observed emission to the QWRs. Thus, carrier confinement in such quantum structures allows us to achieve PL emission energies up to 4.4 eV with the possibility of controlling the QWR emission properties by the geometry of the AlN/GaN NW template and deposition of properly designed capping layers.

D Conclusions

In conclusion, we have demonstrated a significant shift of the UV emission of GaN NWs to higher energies due to the formation of self-assembled GaN QWRs on the 6 edges of hexagonal prismatic GaN–AlN core–shell NW heterostructures. Furthermore, the QWRs present single emission lines with narrow widths (10 meV). QWR growth is initiated by the different nucleation properties of GaN on $\{1\bar{1}00\}$- and $\{11\bar{2}0\}$-facets and the synthesis in a large growth window has been demonstrated by atomic-resolution aberration-corrected HAADF STEM. The presence of the QWRs was also proved by TRPL spectroscopy, which revealed a significantly shorter decay time of about 120 ps compared to the GaN NW emission.

Stabilization by an additional AlN capping layer results in a blue-shift of the emission properties and allows visualization of QWRs with a lateral extension down to 1 ML. The PL emission from single QWRs was analyzed by μ-PL analysis of single NWs and allowed an estimation of the average QWR size assuming a triangular cross-section with the base length being determined by the size of the $\{11\bar{2}0\}$ nucleation facet and the sidewalls being formed by $\{1\bar{1}00\}$-facets according to the suggested model for a self-limiting growth process.

According to the presented results, QWR formation can be expected to occur in all types of PAMBE-grown AlN/GaN (and very likely AlGaN/GaN) NW heterostructures and to have major implication for the growth of non-polar quantum wells using core–shell structures. Due to preferential nucleation on the exposed *a*-plane fragments at the intersections of *m*-plane sidewalls, an inhomogeneous thickness of the radial QW can be inferred. This yields a new technique for the controlled realization of smaller scale quantum objects opening the route to investigate the related novel physical properties in one-dimensional structures. In general, this approach could be extended to other semiconductor materials to help in tuning of energy emission to minimize energy losses.

Acknowledgements

This work was partially supported by the Spanish project Consolider Ingenio CSD2009 00013 IMAGINE. JA acknowledges the funding from the Spanish MICINN project MAT2010-15138 (COPEON), PRI-PIMERU-2011-1422 (InCoSiN) and Generalitat de Catalunya (2009 SGR 770 and NanoAraCat). JRM acknowledges CSD2009 00050 MULTICAT, MAT2010-21510 and ERDF (FEDER Programa Competitivitat de Catalunya). The authors from JLU and WSI acknowledge financial support from the EU within the FP 7 STREP DOTSENSE (Grant no. 224212) and from the German Science Foundation within NAWACS (EI 518/5). The authors from Paris and Giessen acknowledge financial support from the EGIDE and PROCOPE bilateral exchange programs within the project GANOPHOT.

References

1 E. Kapon, D. M. Hwang and R. Bhat, *Phys. Rev. Lett.*, 1989, **63**, 430.
2 W. Wegscheider, L. N. Pfeiffer, M. M. Dignam, A. Pinczuk, K. W. West, S. L. McCall and R. Hull, *Phys. Rev. Lett.*, 1993, **71**, 4071.
3 R. Notzel, N. N. Ledentsov, L. Daweritz, K. Ploog and M. Hohenstein, *Phys. Rev. B: Condens. Matter*, 1992, **45**, 3507; H. Yu, J. B. Li, R. A. Loomis, L. W. Wang and W. E. Buhro, *Nat. Mater.*, 2003, **2**, 517.
4 E. Uccelli, J. Arbiol, J. R. Morante and A. F. I. Morral, *ACS Nano*, 2010, **4**, 5985.
5 Z. Tang, N. A. Kotov and M. Giersig, *Science*, 2002, **297**, 237.
6 F. Wang, V. L. Wayman, R. A. Loomis and W. E. Buhro, *ACS Nano*, 2011, **5**, 5188.
7 H. Yu, L. Jingbo, R. A. Loomis, L. W. Wang and W. E. Buhro, *Nat. Mater.*, 2003, **2**, 517.
8 J. R. Heath and F. K. LeGoues, *Chem. Phys. Lett.*, 1993, **208**, 263.
9 J. D. Holmes, K. P. Johnston, R. C. Doty and B. A. Korgel, *Science*, 2000, **287**, 1471.
10 S. Koshiba, H. Noge, H. Akiyama, T. Inoshita, Y. Nakamura, A. Shimizu, Y. Nagamune, M. Tsuchiya, H. Kano and H. Sakaki, *Appl. Phys. Lett.*, 1994, **64**, 363.
11 H. Fujikura and H. Hasegawa, *J. Electron. Mater.*, 1996, **25**, 619.
12 H. Weman, S. Palmgren, K. F. Karlsson, A. Rudra, E. Kapon, D. L. Dheeraj, B. O. Fimland and J. C. Harmand, *J. Mater. Sci.: Mater. Electron.*, 2009, **20**, 94.
13 P. Kröger, M. Ruth, N. Weber and C. Meier, *Appl. Phys. Lett.*, 2012, **100**, 263114.
14 W. Wegscheider, L. N. Pfeiffera, A. Pinczuka, K. W. Westa, M. M. Dignama, R. Hulla and R. E. Leibenguth, *J. Cryst. Growth*, 1995, **150**, 285.
15 B. Amstatt, J. Renard, C. Bougerol, E. Bellet-Amric, B. Gayral and B. Daudin, *J. Appl. Phys.*, 2007, **102**, 074913.
16 G. Ferrari, G. Goldoni, A. Bertoni and E. Cuoghi, *Nano Lett.*, 2009, **9**, 1631.
17 Y. Li, J. Xiang, F. Qian, S. Gradecak, Y. Wu, H. Yan, D. A. Blom and C. M. Lieber, *Nano Lett.*, 2006, **6**, 1468; M. E. Pistol and C. E. Pryor, *Phys. Rev. B: Condens. Matter Mater. Phys.*, 2008, **78**, 115319; K. Hestroffer, R. Mata, D. Camacho, C. Leclere, G. Tourbot, Y. M. Niquet, A. Cros, C. Bougerol, H. Renevier and B. Daudin, *Nanotechnology*, 2010, **21**, 415702.
18 F. Calle, F. J. Sánchez, J. M. G. Tijero, M. A. Sánchez-García, E. Calleja and R. Beresford, *Semicond. Sci. Technol.*, 1997, **12**, 1396–1403; E. Calleja, M. A. Sanchez-Garcia, F. J. Sanchez, F. Calle, F. B. Naranjo, E. Munoz, S. I. Molina, A. M. Sanchez, F. J. Pacheco and R. Garcia, *J. Cryst. Growth*, 1999, **201**, 296; E. Calleja, M. A. Sánchez-García, F. J. Sánchez, F. Calle, F. B. Naranjo, E. Muñoz, U. Jahn and K. Ploog, *Phys. Rev. B: Condens. Matter*, 2000, **62**, 16826; M. Yoshizawa, A. Kikuchi, M. Mori, N. Fujita and K. Kishino, *Jpn. J. Appl. Phys.*, 1997, **36**, L459.
19 L. Lymperakis and J. Neugebauer, *Phys. Rev. B: Condens. Matter Mater. Phys.*, 2009, **79**, 241308.
20 F. Furtmayr, J. Teubert, P. Becker, S. Conesa-Boj, J. R. Morante, J. Arbiol, A. Chernikov, S. Schäfer, S. Chatterjee and M. Eickhoff, *Phys. Rev. B: Condens. Matter Mater. Phys.*, 2011, **84**, 205303.
21 F. Furtmayr, M. Vielemeyer, M. Stutzmann, J. Arbiol, S. Estradé, F. Peiró, J. R. Morante and M. Eickhoff, *J. Appl. Phys.*, 2008, **104**, 034309.
22 A. F. I. Morral, J. Arbiol, J. D. Prades, A. Cirera and J. R. Morante, *Adv. Mater.*, 2007, **19**, 1347.

23 S. Bernal, F. J. Botana, J. J. Calvino, C. López Cartes, J. A. Pérez Omil and J. M. Rodríguez-Izquierdo, *Ultramicroscopy*, 1998, **72**, 135.
24 J. Arbiol, A. Cirera, F. Peiró, A. Cornet, J. R. Morante, J. J. Delgado and J. J. Calvino, *Appl. Phys. Lett.*, 2002, **80**, 329; E. Uccelli, J. Arbiol, C. Magen, P. Krogstrup, E. Russo-Averchi, M. Heiss, G. Mugny, F. Morier-Genoud, J. Nygard, J. R. Morante and A. F. I. Morral, *Nano Lett.*, 2011, **11**, 3827; E. Russo, M. Heiss, L. Michelet, P. Krogstrup, J. Nygård, J. R. Morante, E. Uccelli, J. Arbiol and A. F. I. Morral, *Nanoscale*, 2012, **4**, 1486.
25 A. Chernikov, S. Horst, M. Koch, K. Volz, S. Chatterjee, S. W. Koch, T. A. Wassner, B. Laumer and M. Eickhoff, *J. Lumin.*, 2010, **130**, 2256.
26 L. Rigutti, J. Teubert, G. Jacopin, F. Fortuna, M. Tchernycheva, A. De Luna Bugallo, F. H. Julien, F. Furtmayr, M. Stutzmann and M. Eickhoff, *Phys. Rev. B: Condens. Matter Mater. Phys.*, 2010, **82**, 235308.
27 J. Teubert, P. Becker, F. Furtmayr and M. Eickhoff, *Nanotechnology*, 2011, **22**, 275505.
28 C. Pfüller, O. Brandt, F. Grosse, T. Flissikowski, C. Cheze, V. Consonni, L. Geelhaar, H. T. Grahn and H. Riechert, *Phys. Rev. B: Condens. Matter Mater. Phys.*, 2010, **82**, 045320.
29 M. de la Mata, C. Magen, J. Gazquez, M. I. B. Utama, M. Heiss, S. Lopatin, F. Furtmayr, C. J. Fernández-Rojas, B. Peng, J. R. Morante, R. Rurali, M. Eickhoff, A. F. I. Morral, Q. Xiong and J. Arbiol, *Nano Lett.*, 2012, **12**, 2579.
30 M. I. B. Utama, F. J. Belarre, C. Magen, B. Peng, J. Arbiol and Q. Xiong, *Nano Lett.*, 2012, **12**, 2146.
31 http://www.icmab.cat/gaen/research/165.
32 F. Furtmayr, M. Vielemeyer, M. Stutzmann and M. Eickhoff, *J. Appl. Phys.*, 2008, **104**, 074309.
33 L. Rigutti, G. Jacopin, L. Largeau, E. Galopin, A. De Luna Bugallo, F. H. Julien, J.-C. Harmand, F. Glas and M. Tchernycheva, *Phys. Rev. B: Condens. Matter Mater. Phys.*, 2011, **83**, 155320.
34 See NEXTNANO website [http://www.wsi.tum.de/nextnano3] for tutorial input files and detailed documentation.

Published on 09 October 2012. Downloaded by UNIVERSITAT GIESSEN on 24/01/2014 13:19:43.

This journal is © The Royal Society of Chemistry 2012